

Microwave Quasi-periodic Pulsations in Multi-timescales Associated with a Solar Flare/CME Event

Baolin Tan¹, Yin Zhang, Chengming Tan, & Yuying Liu

*Key Laboratory of Solar Activity, National Astronomical Observatories
Chinese Academy of Sciences, China*

bltan@nao.cas.cn

ABSTRACT

Microwave observations of quasi-periodic pulsations (QPP) in multi-timescales are confirmed to be associated with an X3.4 flare/CME event at Solar Broadband Radio Spectrometer in Huairou (SBRs/Huairou) on 13 December 2006. It is most remarkable that the timescales of QPPs are distributed in a broad range from hecto-second (very long period pulsation, VLP, the period $P > 100$ s), deca-second (long period pulsation, LPP, $10 < P < 100$ s), few seconds (short period pulsation, SPP, $1 < P < 10$ s), deci-second (slow-very short period pulsation, slow-VSP, $0.1 < P < 1.0$ s), to centi-second (fast-very short period pulsation, fast-VSP, $P < 0.1$ s), and forms a broad hierarchy of timescales. The statistical distribution in logarithmic period-duration space indicates that QPPs can be classified into two groups: group I includes VLP, LPP, SPP and part of slow-VSPs distributed around a line approximately; group II includes fast-VSP and most of slow-VSP dispersively distributed away from the above line. This feature implies that the generation mechanism of group I is different from group II. Group I is possibly related with some MHD oscillations in magnetized plasma loops in the active region, e.g., VLP may be generated by standing slow sausage mode coupling and resonating with the underlying photospheric 5-min oscillation, the modulation is amplified and forms the main framework of the whole flare/CME process; LPP, SPP, and part of slow-VSPs are most likely to be caused by standing fast modes or LRC-circuit resonance in current-carrying plasma loops. Group II is possibly generated by modulations of resistive tearing-mode oscillations in electric current-carrying flaring loops.

Subject headings: Sun: flares — Sun: oscillations — Sun: radio radiation

1. Introduction

Solar quasi-periodic pulsations (QPP) are frequently observed in optical, EUV, radio, soft X-ray, hard X-ray, and even Gamma-ray emissions (Nakariakov et al, 2010). Same as seismological waves can reveal interior structure of the Earth or other celestial bodies, solar QPPs are also a kind of very important phenomena which may provide some information, such as the interior structures and the physical conditions of the source regions or the propagating media. The flare-associated QPP can provide information of solar flaring regions, and give some prospective enlightening of coronal plasma dynamic processes, such as to remote diagnose the microphysics of energy releasing sites. Especially the QPP occurred in microwave frequency range is always regarded as a direct signal of flaring primary energy-releasing regions. So far, from observations we know

¹Datun Road A20, Chaoyang District, Beijing, 100012, China.

the timescales (expressed as period P) of QPPs are in a wide range from a few tens of milliseconds to several minutes. Based on the summary of previous observational and theoretical investigations, according to the timescale of periods, we may extend the previous QPP classification (Wang & Xie, 2000) into a much wider hierarchy:

(1) Very long period pulsation (VLP), which is also named as very low frequency oscillation. Its period is in hecto-second or several minutes. Generally we may define VLP as $P > 100$ s (e.g. 40 min, Kaufmann, 1972; 276 s, Aschwanden et al, 1999; 8 – 12 min, Foullon et al, 2005; 10-18 min, Foullon et al, 2010).

(2) Long period pulsation (LPP). The period is in deca-second, defined as $10 < P < 100$ s (e.g. Parks & Winckler, 1969; Qin et al, 1996; Melnikov et al, 2005; Inglis & Nakariakov, 2009; etc).

(3) Short period pulsation (SPP). This kind of QPP is very popular, and its period is in seconds, $1 \leq P < 10$ s (e.g. Abrami, 1970; Rosenberg, 1970; Trotter et al, 1981; Zaitsev & Stepanov, 1982; Qin et al, 1996; etc).

(4) Very short period pulsation (VSP). Its period is in sub-second. Frequently it is always down to tens of milliseconds (e.g. Young et al, 1961; Gotwols, 1972; Fleishman et al, 2002; Tan et al, 2007; Tan, 2008; Jiricka & Karlicky, 2008; Karlicky, Zlobec, & Meszarosova, 2010; etc), so we may classify VSPs into two sub-classes (Tan et al, 2007):

1) slow-VSP, the period is in deci-second, $0.1 < P < 1.0$ s;

2) fast-VSP, the period is in centi-second, $P < 0.1$ s, usually, it is only several tens of millisecond.

Intrinsically, there is no distinct borderline between different classes of QPPs. So far, because of instrumental limitations, we have not distinguished any QPPs with period of shorter than 10 milliseconds reliably.

In previous studies, there is always only one or two classes of QPPs reported in one flare event. Even if the multi-periodic pulsations observed in some cases, they are also only with one or two classes of QPPs. For example, in the work of Qin et al (1996), the periods of the two pulsating components are 1.5 s and 40 s which are belonging to SPP and LPP, respectively; in the work of Melnikov et al (2005), the periods of two pulsating components are 14 – 17 s and 8 – 11 s, respectively, which are ranked in same class of QPP; in the work of Inglis & Nakariakov (2009), the periods of three pulsating components are 28 s, 18 s, and 12 s, respectively, and all of them are belonging to one and the same class of LPP. Karlicky et al (2005) reported the timescales of slowly drifting pulsating structures (DPS) with period of 0.9–7.5 s, and the short periods presents as a power-law distribution, especially in the range of 0.06-0.2 s, where the power-law index is in the range of 1.3-1.6. So far we have no literatures to show the coexistence of more than two different classes of QPP in a same flaring event. We do not know what is the relationship among different classes of QPPs. At the same time we have plenty of reasons to suppose that such relationships may imply some physical information of the solar active region or the flaring mechanisms.

It is very luck that an X3.4 flare/CME event occurred in solar active region of AR 10930 on 2006 December 13. This event has many unusual features: (1) AR 10930 is an isolated active region on the solar disk (Left panel of Fig.1); (2) the flare is a long duration event, the GOES soft X-ray bursts start at 02:14 UT and end at 02:57 UT, and the radio bursts start at 02:20 UT and last to after 04:50 UT; (3) the eruption is repetitious, from broadband microwave observations, we may find that this event has many big bursts clearly. Many people studied this flare/CME event from different points of view (Kosovichev & Sekii, 2007; Yan, et al, 2007; Ning, 2008; Kuznetsev, 2008; Zhang et al, 2008; etc). Especially, in the work of Minoshima

et al (2009), they presented multi-wavelength observations of electron acceleration in the flare. And in the Fig.1 of their paper, the light curves of microwave radio emission observed at NoRP (9.4 GHz, 17 GHz, and 34 GHz) and hard X-ray obtained at RHESSI in 25 – 40 keV, 40 – 60 keV demonstrate quasi-periodic pulsations with very long period. Together with the great number of very short period pulsations (VSP) observed in Chinese Solar Broadband Radio Spectrometer (SBRS/Huairou) (Tan et al, 2007; Tan, 2008), it is rational to investigate the observations of QPPs in multi-timescales, their mutual relationships, and the possible physical implications in detail. From these investigations, we find that the most remarkable feature in this flare event is the coexistence of several classes of QPPs, including VLP, LPP, SPP, slow-VSP and fast-VSP, and these QPPs form a broad hierarchy of timescales.

In this work, based on the observations at frequency of 2.60 – 3.80 GHz at SBRS/Huairou, we present the observations and analysis of multi-timescales in QPPs associated with the flare event on 2006 December 13. Section 2 is an introduction of the observation data and analysis methods. Section 3 presents the main features of QPPs. In section 4 we give a detailed discussion of physical mechanisms of QPPs with multi-timescales. Finally, there is a summary and some deductions in section 5.

2. Observations Data and Analysis

2.1. Observation Data

The X3.4 flare/CME event in AR 10930 on 2006 December 13 is observed by RHESSI, Hinode, NoRH, NoRP, SOHO/MDI, TRACE and SBRS/Huairou, etc (Kubo et al, 2007; Su et al, 2007; et al). We select mainly the observations of SBRS/Huairou because of its high cadence, broad frequency bandwidth, and high frequency resolution, to investigate the multi-timescale pulsating phenomena associated with the flare/CME event. SBRS/Huairou includes 3 parts: 1.10-2.06 GHz, 2.60-3.80 GHz, and 5.20-7.60 GHz (Fu et al 1995; Fu et al 2004; Yan et al, 2002). However, only the spectrometer of 2.60 – 3.80 GHz is operating well around the above flare/CME event. The diameter of the antenna of the spectrometer is 3.2 m. The antenna points to the center of solar disk automatically controlled by a computer. The spectrometer can receive the total flux of solar radio emission with dual circular polarization (left- and right circular polarization), and the dynamic range is 10 dB above quiet solar background emission. And the observation sensitivity is: $S/S_{\odot} \leq 2\%$, here S_{\odot} is quiet solar background emission. Similar to other several spectrometers, such as Phoenix (100 – 4000 MHz, Benz et al, 1991), Ondřejov (800 – 4500 MHz, Jiricka et al, 1993) and BBS (200 – 2500 MHz, Sawant et al, 2001), SBRS/Huairou have no spatial resolution. However, a great deal of works (e.g. Dulk, 1985, etc) show that the radio bursts received by spectrometers are always coming from the solar active region when the antenna points to the Sun. In this work, because AR 10930 is an isolated active region around the X3.4 flare/CME event (shows in the left panel of Fig.1), we believe that the microwave bursts are just coming from the same active region associated with the event. In the frequency range of 2.60 - 3.80 GHz, there are 120 channels with frequency resolution of 10 MHz, temporal resolution of 8 ms, left- and right-circular polarization components with accuracy of polarization degree 5 – 10 %. The data were analyzed by using a software that was developed with IDL algorithm. In order to identify weak burst structures, some wavelet methods have been developed for data processing. The calibration of the observation data is followed a method proposed by Tanaka et al (1973). The standard flux values of the quiet Sun is adopted the data published by Solar Geophysical Data (*SGD*) at frequencies 4995 MHz, 2800 MHz, 2695 Mhz and 1415 Mhz. As for strong bursts, the receiver may work beyond its linear range and a nonlinear calibration method will be used instead (Yan et al, 2002).

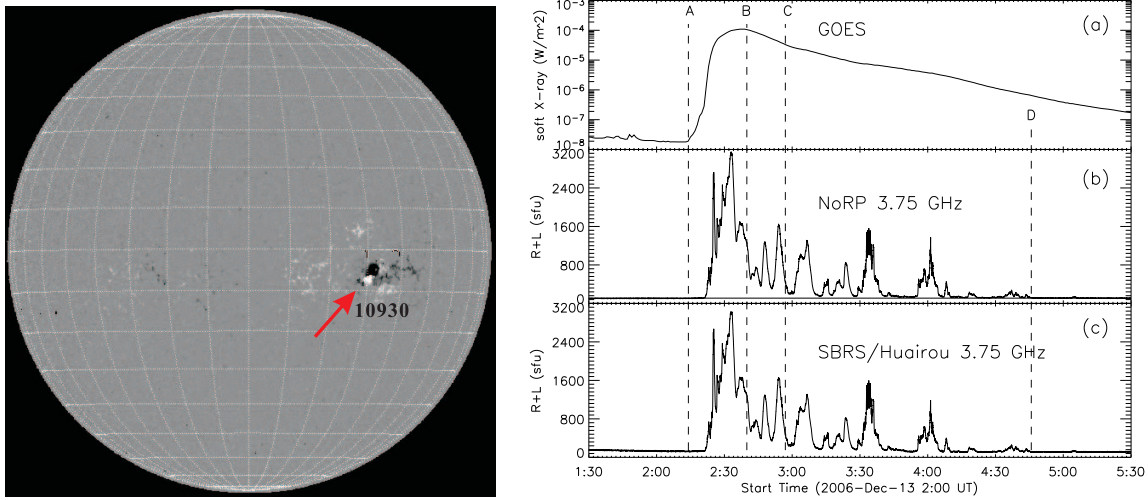


Fig. 1.— Left panel is a full-disk longitudinal magnetogram taken by MDI/SOHO on 13 Dec. 2006. The right panel presents observation comparisons between solar soft X-ray intensity taken by GOES satellite (a), radio emission intensities at frequency of 3.75 GHz taken by NoRP (b, in Japan) and SBRS/Huairou (c, in China) at 01:30 – 05:30 UT, 13 Dec. 2006. The dashed vertical lines marked as A, B, C and D indicate the start, peak, end time of the soft X-ray flare observed by the GOES, and the end time of the radio burst, respectively.

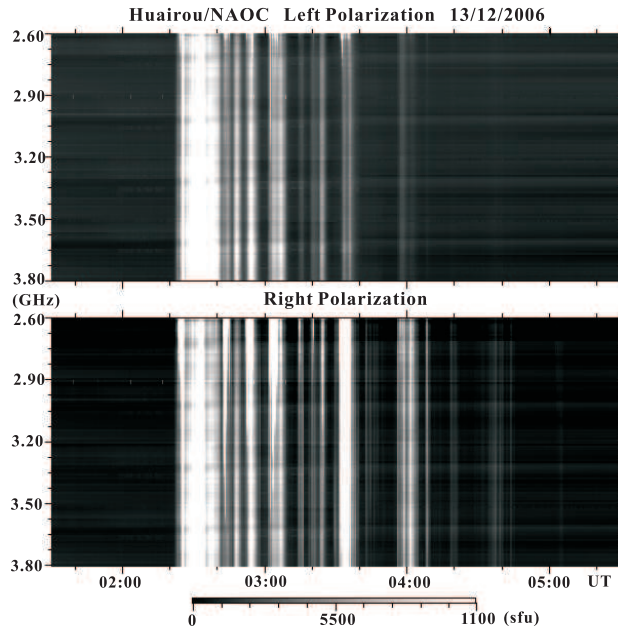


Fig. 2.— Spectrogram of the solar radio emission at frequency of 2.60 – 3.80 GHz at 01:30 – 05:30 UT, 13 Dec. 2006.

In order to confirm that the observations of SBRS/Huairou are not artificial, we make comparisons among SBRS/Huairou, Nobeyama Radio Polarimeters (NoRP) and soft X-ray intensity obtained at GOES satellite. Here, NoRP is observing the Sun with multiple frequencies 1.0, 2.0, 3.75, 9.4, 80 GHz. It is capable to obtain solar total flux and circular-polarization degree with temporal resolution of 0.2 s. The right panel of Fig.1 presents the observed results of GOES soft X-ray intensity (a), radio emission intensities obtained at NoRP (b) and SBRS/Huairou (c) at the same frequency of 3.75 GHz at 01:30 – 05:30 UT, 13 Dec. 2006. We find that these radio results obtained from the two different telescopes (one is in China, and the other is in Japan) are almost selfsame in profile shape and intensity. Fig.2 presents the dynamic spectrogram of solar radio emission at frequency of 2.60 – 3.80 GHz at 01:30 – 05:30 UT, 13 Dec. 2006. Radio bursts start (02:20 UT) after the flare onset (02:14 UT), and end at 04:50 UT. They are consistent with the enhancement of GOES soft X-ray intensity. These facts confirm again that radio observations of SBRS/Huairou are coming from the solar flaring processes.

The most advantage of SBRS/Huairou is that it is possible to provide much of peculiar information synchronously, such as polarization degree, pulsating frequency bandwidth, frequency drifting rate, and fine structures of microwave emission spectrograms with much higher temporal and frequency resolutions than most other instruments.

2.2. Analysis Method

As a rule, we can use Fourier analysis (Fast Fourier Transformation, FFT) or wavelet analysis to investigate pulsating structures in observation data. Generally, QPP always behaves as a train of approximated paralleled vertical and equidistant stripes in broadband dynamic spectrograms. Each stripe represents one pulse. The time interval between two adjacent strips represents the pulsating period. By scrutinizing observed dynamic spectrograms, we can also distinguish and confirm the existence of QPPs clearly, and pickup their parameters easily, such as central emission frequencies (f_0), frequency bandwidth (b_w), period (P), duration (D), global frequency drifting rate (R_{gfd}), signal pulse frequency drifting rate (R_{spfd}), and polarization degree (r), etc. In a QPP, parameters of P , f_0 , b_w , r , R_{gfd} and R_{spfd} may have alike values. In different QPP, the above parameters will have obviously different values. We can easily distinguish one QPP from the others. Then we need to decompose pulsating components from the observed data. In our observations, the data have two modes synchronously: one is with cadence of 0.2 s, and the other has cadence of 8 ms. From observations with cadence of 0.2 s, we may investigate features of VLP, LPP and part of SPP; and from the observations with cadence of 8 ms, we may investigate VSP and most of the SPP.

In order to make the pulsating component more clearly and reliably, we adopt two methods to investigate QPPS. These two methods can be cross-examined mutually. When their results are consistent with each other, a QPP is identified. The first method is Fourier analysis (Fast Fourier Transformation, FFT) with observed data. The second method is a kind of statistical method, which directly counts the temporal intervals between adjacent pulse peaks in the pulsating structures from the broadband radio dynamic spectrogram. This method is very straightforward, the details is presented in following paragraphs.

(1) Identify solar microwave bursts. Because the instrument sensitivity is $S/S_{\odot} \leq 2\%$. From SGD data, we may get the microwave flux intensity of the quiet solar background emission at frequency 2.695 GHz, 2.800 GHz, and 4.995 GHz are 52 sfu, 88 sfu, 90.7 sfu, and 158 sfu, respectively, on 2006 December 13. Then we may obtain the microwave flux intensity of quiet solar background emission at each frequency channel in the range of 2.60 – 3.80 GHz is 85.3 – 121.4 sfu by linear extrapolation, and the instrument sensitivity

is about 1.70 – 2.40 sfu. More securely, when the microwave flux intensity is 5.0 sfu (more than 2 times instrument sensitivity in frequency 2.60 – 3.80 GHz) higher than the quiet solar background emission, we may confirm the existence of a solar microwave burst.

(2) Identify pulsating structure by scrutinizing the observed spectrograms directly. Here, the microwave flux intensity at each pulse in pulsating structure will be 5.0 sfu higher than the quiet solar background emission, so it is very clear in dynamic spectrogram.

(3) Obtain the timescale of pulsating structure approximately by direct counting the temporal intervals between adjacent pulse peaks from the spectrogram. Such estimation can give roughly values of period P' , duration D , central emission frequency f_0 , and the bandwidth b_w of QPP.

(4) Smooth the observing flux curves to filter out the high frequency noise components by using a sliding window narrower than pulsating period, the result may be expressed as F . The width of the smoothing window should be exponentially as $\frac{1}{4}P'$.

(5) Smooth the flux curves F in a wide sliding window to filter out the pulsating component and obtain the background emission of QPP. The width of the smoothing window should be exponentially as $2P'$. The result can be expressed as F_b . Generally, the background emission during the flare/CME event is much greater than the quiet sun emission (before the event, i.e. before 02:20 UT), and it equals to quiet sun emission before the flare event.

Usually, the smoothing method will generate some additionally boundary effects. In order to suppress such effects, we need to extend the range of the analyzing data. That is to say, if the duration of QPP is D , the QPP starts from t_1 and ends at t_2 , $D = t_2 - t_1$, then we select the analyzing data from $t_1 - \frac{1}{2}D$ to $t_2 + \frac{1}{2}D$ before make smoothing processing. After smoothing processing, we investigate the pulsating features only within the data fragment from t_1 to t_2 .

(6) Subtract the background emission F_b from the result F of step (4) and obtain the pulsating component (F_p), $F_p = F - F_b$. So, the pulsating component is a quantity relative to the background emission F_b , it will oscillate from positive to negative values around F_b .

(7) Investigate the dynamic features of QPPs by analyzing F_p . Such features may include more exact period P , modulation degree M , polarization degree r , single pulse frequency drifting rates R_{spfd} , and global frequency drifting rate R_{gfd} . These parameters are defined and explained in paper of Tan (2008).

Fig.3 presents an example of the above QPP extraction procedure. Here, we note that the existence of saturation effects at several segments may affect the analysis results. Such saturation effects exist at 02:25 – 02:25:30, 02:41:30-02:43, 02:52 – 02:54, 03:01:40 – 03:05, and 03:32 – 03:36. Additionally, from the above method, the pulsating component (F_p) is a quantity relative to the background emission (F_b), and F_b is an average level by smoothing the flux curves (F) in a wide sliding window. From the left panel of Fig.3 we know that F_b is much greater in the flare/CME event than the quiet sun emission (before the event, i.e. before 02:20 UT), it is possibly mainly associated with thermal plasmas in the flaring region. So the actual radiation flux in QPP is always positive. The negative F_p is only a relative result respect to F_b .

3. Main Features of QPPs

Based on the above observation data and analysis methods, we find that there are 5 classes of QPPs, including VLP, LPP, SPP, slow- and fast-VSP, coexisting associated with the flare/CME event on 13 De-

ember, 2006. They form a broad hierarchy of QPPs with different timescales. All the QPPs are occurred during the enhancement of soft X-ray obtained by GOES satellite. From the right panel of Fig.1 we find that there is no radio burst occurred before 02:20 UT and after 04:50 UT, and the dynamic spectrogram in Fig.2 is almost uniform pattern during these two time sections. We also use Fourier analysis to these two sections of observation data, and find no pulsating evidence. These facts indicate that there is no detected pulsating structures before and after the flare/CME event. All the QPPs are associated with the above mentioned flare/CME event.

3.1. Very Long-period Pulsation (VLP)

The most remarkable implication of Fig.1, Fig.2, and Fig.3 may be the quasi-periodic pulsations with very long-periods. According to the profile, the radio bursts can be plotted into 4 paragraphs of QPP which marked as A, B, C, D, and separated by vertical dash-dotted lines in Fig.3, respectively.

The left panel of Fig.4 is pulsating components at different frequencies of the VLP including paragraph A and B occurred at 02:20 – 03:50 UT, 13 Dec. 2006 at frequency of 2.60 – 3.80 GHz, which indicates that the VLP is a broadband pulsation and goes beyond the possible frequency range of the telescope. The solid and dotted curves represent the right and left circular polarized component, respectively. Values of pulsating components are relative to the background emission F_b . There are 18 pulses in these paragraphs. The magnitudes of the pulsating emission flux at each pulse are in the range of 200 – 1100 sfu at both circular polarizations. The right panel is a result of Fourier analysis (FFT) at frequency of 2.95 GHz, the peak indicates that the period is 258 s.

In fact, there is an obviously gap between pulse 8a and 1b which divides them into 2 paragraphs:

Paragraph A includes pulses numbered as 1a – 8a (vertical dot-dashed lines) with period of 3.1 – 5.8 minutes. According to the Fourier analysis we may obtain the period is about 248 s (about 4.1 minutes). The averaged magnitudes of the pulsating emission flux is about 350 sfu. However, there are several pulses (pulse 2a, 3a and 6a), of which values of the pulsating emission flux are disturbed by saturation effects, and this make the analysis with some uncertainties that we can not get a reliable trend from pulse 1a to 8a.

Paragraph B includes pulses numbered 1b – 10b (vertical dotted lines) at 03:01 – 03:45 with period of 4.0 – 5.1 minutes, and from the Fourier analysis we may obtain the period is about 270 s (4.5 minutes). The averaged magnitudes of the pulsating emission flux is about 300 sfu. The saturation effect is also disturbed pulses 1b and 8b in same way. However, we can also get the trend that the magnitudes of the pulses increase from 1b to 8b, and then decrease from 8b to 10b. Straightforwardly, the periodicity of paragraph B is more stable than that of paragraph A. At the same time, the magnitude of the pulsating emission flux at each pulse in paragraph A is higher than that in paragraph B.

As we mentioned above, the time intervals between two adjacent pulses on the QPP structure can represent the period of QPP. Fig.5 presents the evolution of these time intervals in VLP paragraph A (in panel a) and B (in panel b). We may find that the period of paragraph A increases from about 3 min at the beginning to about 5.8 min at the end, and the period of paragraph B increases slowly from about 4 min at the beginning to about 5.1 min at the end. This slowly increasing is consistent with the evolution of MHD wave mode under coronal conditions at quasi-periodic phase (Roberts & Edwin, 1984).

The main difference between the two paragraphs is the evolution of polarization degree. The left panel of Fig. 4 gives some evidence that there is a circular polarization reversion from right circular polarization

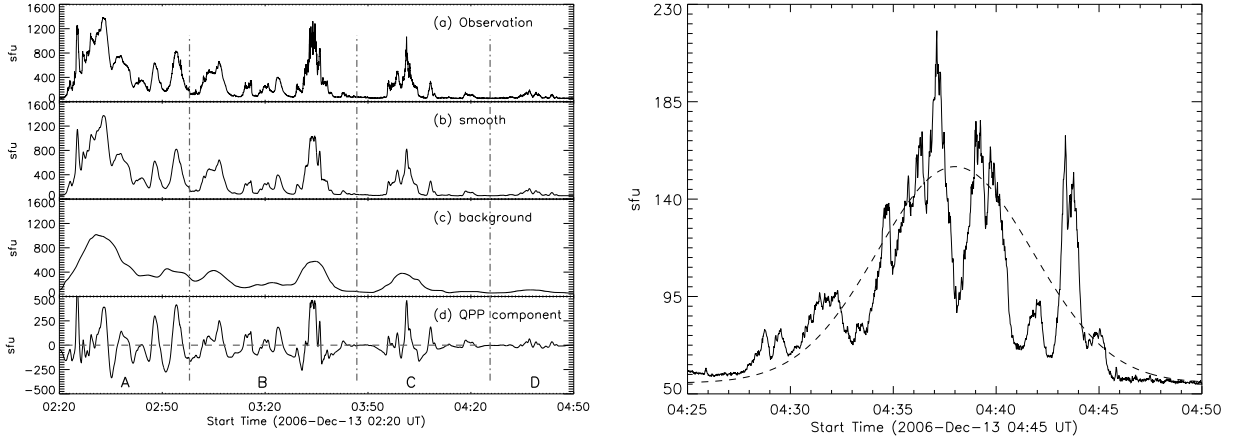


Fig. 3.— Left panel presents the procedure of QPP extractions. (a) is the observational result, (b) is the smoothed result which filter out the high frequency noise components, (c) is the background emission of QPP, and (d) is the pulsating component. According to the profiles, the radio bursts can be plotted into 4 paragraphs of QPP which marked as A, B, C, D, and separated by vertical dash-dotted lines, respectively. The right panel presents the evolution of VLP paragraph D, here the dashed curve is a Gaussian fitted result.

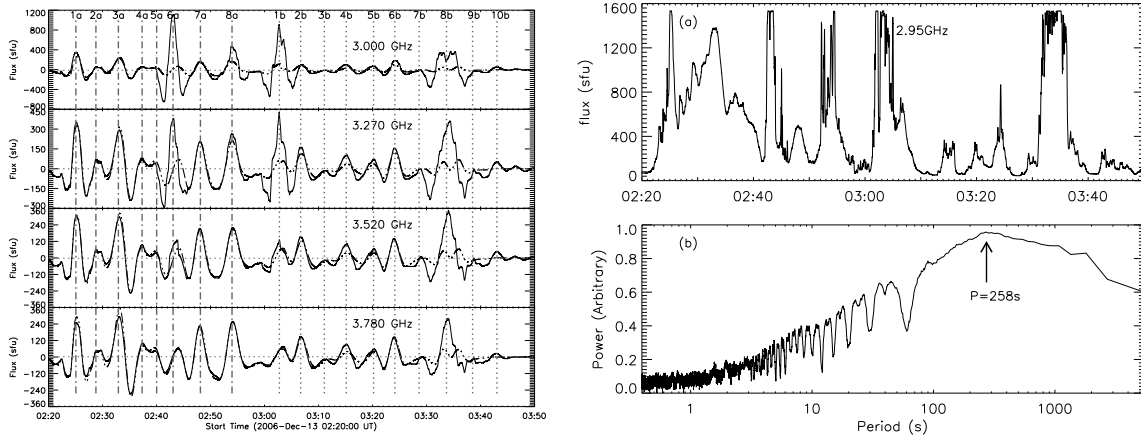


Fig. 4.— VLP occurred at 02:20 – 03:50 UT, 13 Dec. 2006 at frequency of 2.60 – 3.80 GHz observed at SBR/S/Huairou. Left panel is pulsating components at different frequencies. The solid and dotted curves represent the right and left circular polarized component, respectively. Values of pulsating components are relative to the background emission F_b . In right panel (a) is a profile of radio emission at frequency 2.95 GHz. (b) is a result of Fourier analysis (FFT) at the corresponding frequency, which indicates the period of the LPP is 258 s.

to left circular polarization around the frequency of 3.40 GHz in paragraph A. However, in paragraph B, there is no such revisions, and the polarization degree is keeping positive. However, because of saturation effects on both paragraph A and paragraph B, we have no strictly proof to distinguish paragraph A from paragraph B.

Fig.3 presents two other paragraphs of VLP after 03:50 UT: paragraph C starts at 03:56 and ends at 04:22 UT, the period is about 260 s (4.3 min), and the averaged magnitude of the pulsating emission flux is about 200 sfu; paragraph D starts at 04:28 and ends at 04:47., the period is about 220 s (3.7 min), and the averaged magnitude is about 90 sfu, and behaves strongly right circular polarization. This paragraph has no saturation effect, the right panel of Fig.3 presents its magnitude evolution, the dashed curve is a Gaussian fitted result. It shows that the pulsating process increases gradually, reaches to a maximum, and then decreases.

As a whole, from paragraph A, B, C to D, the averaged magnitude of the pulsating emission flux decreases from 350 sfu to 90 sfu, gradually. The period reaches to the maximum (270 s) at paragraph B, and then decreases gradually to a minimum (220 s) at paragraph D.

In addition, there is an obvious frequency drifting at each pulse in VLP (R_{spdf}). Fig.6 presents an example of a method to calculate the single pulse frequency drifting rate of QPP. The dot-dashed line denotes the time of the maximum flux intensity at each frequency, its slope presents the frequency drift rate (R_{spdf}) is about -175 MHz/s. Using this method, we obtained R_{spdf} at each pulse of paragraph A as 21, 47, -183, -440, -215, 55, -175, 50 MHz/s, and at each pulses of paragraph B as 25, 48, 65, 389, 46, -50, -76, 313 MHz/s, respectively. In addition, we can also find that R_{spdf} begins from a positive value, then decreases to negative value, and ends with another positive value in each paragraph. Using the same method, single pulse frequency drifting rates of paragraph C and D are in the range of -50 – ~ 190 MHz/s and -135 – ~ 265 MHz/s, respectively. The main properties of VLPs are summarized in Table 1.

Comparing VLP paragraph A with the Fig.2 of Minoshima et al (2009), we find that its flux profile is very similar to the microwave light curves of 9.4 GHz, 17 GHz, and 34 GHz taken with Nobeyama Radio Polarimeter (NoRP) and the hard X-ray light curves in 25-40 keV, 40-60 keV, and 60-100 keV energy band taken with Reuven Ramaty High Energy Spectroscopic Imager (RHESSI). These facts may indicate that pulsating microwave emissions is most possible to be associated strongly with the non-thermal energetic electrons.

3.2. Long-period Pulsation (LPP)

During the flare/CME event, we totally distinguish 4 segments of LPP listed in Table 1. Fig.7 shows an example of LPP occurred at 02:26 – 02:40 UT, 13 Dec. 2006 observed at SBRS/Huairou. The left panel of Fig.7 is the dynamic spectrogram which indicates the period (the time interval between adjacent pulse stripes) is in the range of 55-95 seconds, with the average of about 70 seconds. In right panel of Fig.7, (a) is the profile of radio emission at frequency 2.84 GHz, the dashed curve is a Gaussian fitted result which shows the magnitude evolution of increasing to a peak and then decreasing, (b) is a result of Fourier analysis (FFT) at the corresponding frequency, which indicates the period of the LPP is 70 s, agreeing with the dynamic spectrogram. The magnitude of the pulsating emission flux at each pulse is in the range of 70 – 220 sfu at both circular polarization components with the polarization degree of about 10 ~ 20%. And the emission bandwidth is also beyond the two borders of the frequency range of the telescope of 2.60 – 3.80 GHz, which is similar to that of VLP.

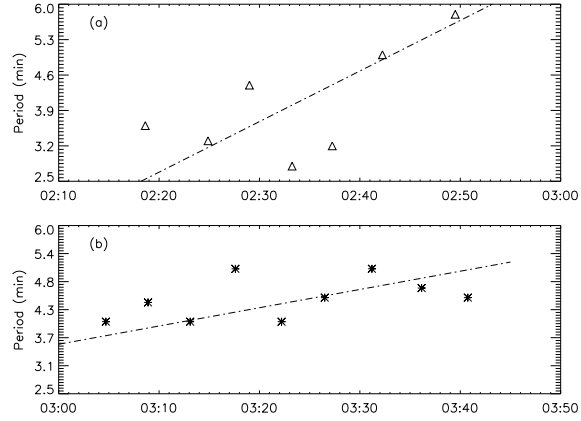


Fig. 5.— Evolution of the time intervals between adjacent pulses in VLP paragraphs. (a) is in paragraph A, and (b) is in paragraph B. the dot-dashed lines are linear squared fitted results.

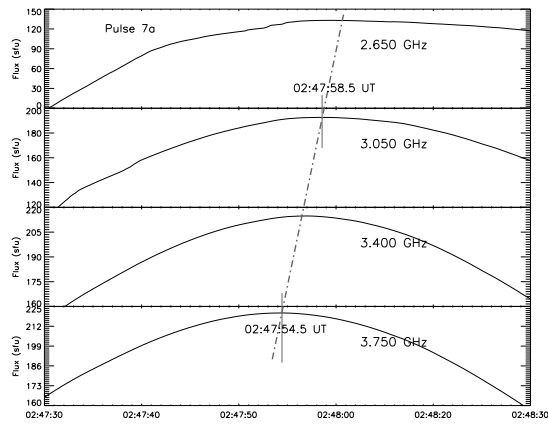


Fig. 6.— Drifting characteristics of a very long period pulsation (here is an example from the pulse 7a marked in the left panel of Fig 4), the dot-dashed line indicates positions of the maximum flux intensity at each curve, and its slope indicates the frequency drift rate at the corresponding pulse.

The other LPPs occurred at 02:38:50 – 02:40:00 with mean period of 16 s (and this LPP has some superfine structures, we will discuss them in the following sections, see Fig.11), at 02:52 – 02:55 UT with mean period of 35 s, and at 03:23:35 – 03:24:50 with mean period of 15 s. Q-factors of these four LPPs are around 5-7 which is approximately a constant.

Using the same method presented in Fig.6, we also find that single pulse frequency drift rate exists in LPP. The average value in these 4 segments are -610 MHz/s, -5.8 MHz/s, -205 MHz/s, and 78.5 MHz/s, respectively. And these values are in the same order as VLP. From the comparison between VLP and LPP we find that there are several points of similarity: analogous frequency bandwidth, single pulse frequency drift rates, polarization degree, and Q-factors. These similarities imply that VLP and LPP should be associated originally with each other.

3.3. Short-period Pulsation (SPP)

During the flare/CME event, we identified 3 segments of SPP. They are listed also in Table 1. Fig.8 presents an example of SPP occurred at 02:59:20 – 03:00:20 UT, 13 Dec. 2006. The left panel of Fig.8 is the dynamic spectrogram which indicates the period (the time interval between adjacent pulse stripes) is in the range of 4.7 – 7.2 s, with the average of 6.2 s. In right panel of Fig.8, (a) is the profile of radio emission at frequency 2.95 GHz, the dashed curve is a Gaussian fitted result which shows the magnitude evolution which also behaves as increasing to a peak and then decreasing, (b) is a result of Fourier analysis (FFT) at the corresponding frequency, which indicates the period of the SPP is 6 s, consistent with the result of dynamic spectrogram. The emission frequency bandwidth is about 600 – 900 MHz, which is narrower than that of VLP and LPP. The magnitude of pulsating emission flux at each pulse is in the range of 40 – 115 sfu with right circular polarization, while there is almost no pulsating component in the left circular polarization. From the dynamic spectrogram, we may also find that SPP has a strong right circular polarization. Additionally, there are obviously frequency drifts at each pulse of the SPP, its value is in the range of -4.0 GHz/s to 3.5 GHz/s. And this frequency drift rate is very close to the drifts of type III bursts (Ma et al, 2006). However, the work of Aschwanden & Benz (1986) indicates that the frequency drift rates of QPPs are considerably different from type III bursts in the similar frequency range, and these two kinds of microwave fine structures are intrinsically different from each other.

In fact, from the dynamic spectrogram of Fig.7 we may find that there is a SPP superposed on the LPP at 02:27:50 – 02:28:20 UT in the frequency range of 2.60 – 3.00 GHz with bandwidth 400 MHz, its period is about 8.0 seconds, and the polarization degree is about 65 – 85%. And the magnitude of the pulsating emission flux at each pulse is in the range of 50 – 120 sfu. The single pulse frequency drift rate is about from -1.5 GHz/s to 2.5 GHz/s. Another SPP occurred at 02:24:35 – 02:24:47 UT with the averaged period of about 1.2 seconds at frequency of 2.60 – 2.95 GHz, the bandwidth is about 350 MHz, and the single pulse frequency drift rate is about 5.0 GHz/s. From these facts we may find that SPP is completely different from VLP and LPP with parameters of polarization degree, frequency drift rate, and frequency bandwidth, etc. These differences imply that SPP may have a different generation mechanism from VLP or LPP.

3.4. Very Short-period Pulsation (VSP)

More than 40 cases of VSP with period $P < 1.0$ s in the frequency range of 2.60 – 3.80 GHz associated with the flare/CME event on 13 December 2006 were reported in the work of Tan et al (2007) and Tan

Table 1: List of VLP, LPP, and SPP occurred in the flare event on 2006-12-13. f_0 , D, P, r, R_{spdf} , and b_w are central frequency, duration, average period, polarization degree, average single pulse frequency drifting rate, and frequency bandwidth, respectively.

| Class | Time (UT) | $f_0(MHz)$ | D(s) | P(s) | r(%) | $R_{spdf}(MHz/s)$ | $b_w(MHz)$ |
|-------|-------------------|------------|------|------|----------|-------------------|------------|
| VLP | 02:23–02:56 | 3200 | 1980 | 248 | 8 ~ 10 | -440~ 55 | >1200 |
| | 03:01–03:45 | 3200 | 2640 | 270 | 8 ~ 12 | -76 ~389 | >1200 |
| | 03:56–04:22 | 3200 | 1560 | 260 | 15 ~ 35 | -50 ~190 | >1200 |
| | 04:28–04:47 | 3200 | 1140 | 220 | 25 ~ 40 | -135 ~265 | >1200 |
| LPP | 02:26–02:34 | 3200 | 480 | 70 | 10 ~ 20 | -610 | >1200 |
| | 02:38:50–02:40:00 | 2800 | 70 | 16 | 10 ~ 20 | -5.8 | 300 |
| | 02:52–02:55 | 3200 | 180 | 35 | 45 ~ 65 | -205 | >1200 |
| | 03:23:35–03:24:50 | 3200 | 75 | 15 | 55 ~ 75 | 78.5 | >1200 |
| SPP | 02:27:50–02:28:20 | 2850 | 30 | 8.0 | 65 ~ 85 | -1500~2500 | 400 |
| | 02:59:20–03:00:20 | 3050 | 60 | 7.5 | 80 ~ 95 | -4000~3500 | 750 |
| | 02:24:35–02:24:47 | 2800 | 12 | 1.2 | 85 ~ 100 | ~5000 | 350 |

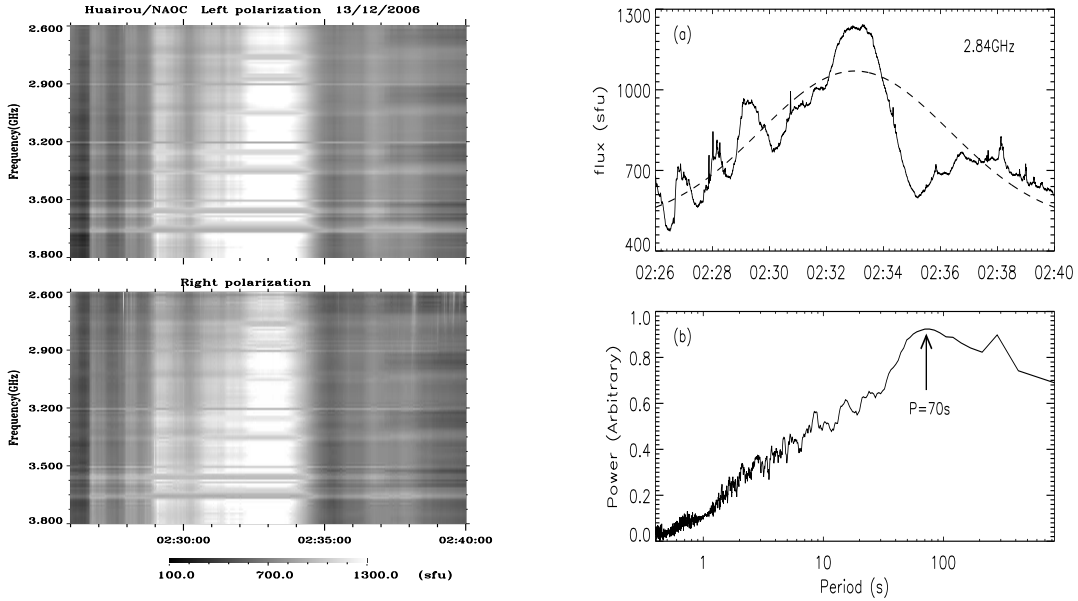


Fig. 7.— The left panel is a spectrogram of a LPP. In right panel, (a) is the profile of radio emission at frequency 2.84 GHz, the dashed curve is a Gaussian fitted result. (b) is the result of Fourier analysis (FFT) at the corresponding frequency, which indicates the period of the LPP is 70 s.

(2008). These VSPs are quasi-periodic, broad bandwidth, and ubiquitous in all phases of the flare/CME event. Among these VSPs, the right circular polarization is very strong. Table 2 of Tan (2008) lists all their observable features. From that list we may classify them into 2 sub-classes:

1) slow-VSP, the period is in deci-second, $0.1s < P < 1.0s$. The left panel of Fig.9 is an example of slow-VSP occurred at 03:25:40 – 03:25:47 UT, 13 Dec. 2006 at frequency of 2.60 – 2.90 GHz. Totally there are 10 slow-VSP cases distinguished from the observations, which are associated with the flare event. And all of them occurred after the flare peak. The period of slow-VSP is in the range of 110 – 416 ms. The duration of each slow-VSP is in the range of 2.2 – 23 s, the single pulse frequency drift rate is in the range of 6.5 – 20 GHz/s and is always positive, the emission frequency bandwidth is in 250 – 700 MHz. The polarization is very strong, similar to that of SPP. The magnitude of the pulsating emission flux is in the range of 20 – 95 sfu. We may also obtain the global frequency drift rate of slow-VSP, and the value is from -31.4 MHz/s to 32.5 MHz/s.

The left panel of Fig.9 shows that the magnitude of pulses increases gradually, and the period decreases from 480 ms to 310 ms slowly. However, the spectrogram becomes continuum after 03:25:47 UT. The possible reason is that it is mixed by some other emissions, and the left panel of Fig.9 is only a partial section of the slow-VSP. By scrutinizing other slow-VSPs, we find that some of them have increasing magnitudes and decreasing periods, and the others have decreasing magnitudes and increasing periods.

Jiřička & Karlický (2008) also found a similar slow-VSP with the period of about 150 ms and the single pulse drift rate is about -17 GHz/s associated with another solar flare event.

2) fast-VSP, the period is in centi-second, $P < 0.1s$. The right panel of Fig.9 is an example of fast-VSP occurred at 03:25:25 – 03:25:29 UT, 13 Dec. 2006 at frequency of 2.60 – 2.90 GHz. There are more than 30 fast-VSPs distinguished from observations associated with the flare event, and they occurred in all phases of the flare (including the rising, peak, vale, and decaying phases). The period of fast-VSP is in the range of 31 – 90 ms. The duration of each fast-VSP is in the range of 2.3 – 16 s, the single pulse frequency drift rate is from 8.33 GHz/s to >30 GHz/s, the emission bandwidth is in 220 – 400 MHz. The polarization degree is slightly higher than that of slow-VSP. The magnitude of the pulsating emission flux is in the range of 15 – 70 sfu, slightly less than that of slow-VSP. The global frequency drift rate of the pulsating event is from -86.2 MHz/s to 34.6 MHz/s, which is very analogous to that of slow-VSP.

The right panel of Fig.9 presents that the magnitude of pulses increases slowly from 160 sfu to a peak of 264 sfu, and then decreases to 145 sfu, and the period increases slowly from 75 ms to 104 ms. Statistically analyzing other fast-VSP, we find that there are 35% fast-VSPs have the above evolutions, and 37% fast-VSPs have evolution of increasing magnitudes and decreasing periods, and 28% fast-VSPs have evolution of decreasing magnitudes and increasing periods. This implies that most of the fast-VSPs are possibly also partially sectional.

Let us come back to the Table 2 in the paper of Tan (2008), we may find that emission frequency bandwidths of the most VSPs are narrower than that of VLP and LPP. Additionally, from the characteristics of the flux profiles, we find that there is another interesting feature: the VSPs can be classified into two classes by another criteria:

1) Ordinary VSP, the width of pulses at half maximum (W_p) is approximated to a half of the gap between two adjacent pulses (W_g): $W_p \approx 0.5W_g$. Most of the fast-VSPs belong to ordinary VSP (see the right panel of Fig.9). In a standard sinusoidal curves: $W_p = \frac{1}{2}W_g$. The ordinary VSPs are sinusoidal-like pulsations.

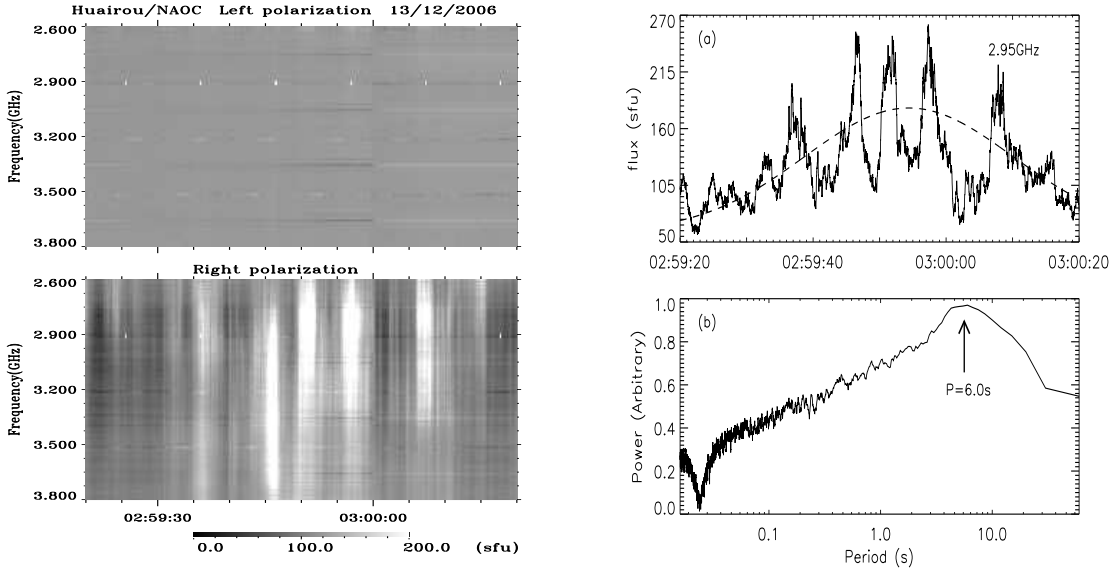


Fig. 8.— Left panel is a spectrogram of a SPP example. In right panel, (a) is the profile of radio emission at frequency 2.84 GHz, the dashed curve is a Gaussian fitted result. (b) is the result of Fourier analysis (FFT) at the corresponding frequency, which indicates the period of the SPP is 6 s.

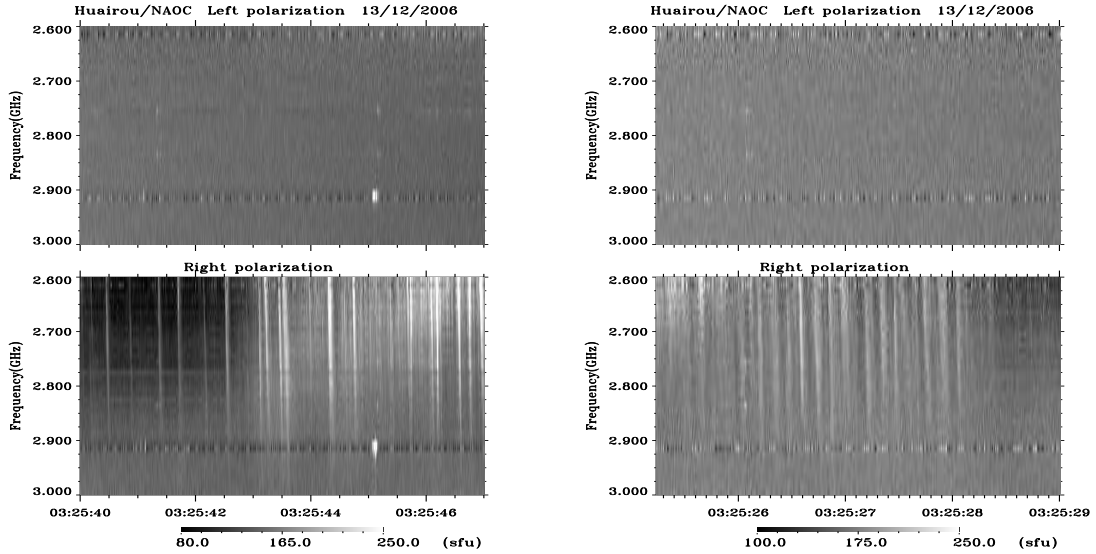


Fig. 9.— Examples of a slow-VSP (extraordinary VSP), and a fast-VSP (ordinary VSP). In each panel, the upper and the lower part is the left- and right- circular polarization component, respectively.

2) Extraordinary VSP, $W_p \ll W_g$. The left panel of Fig.9 shows an example of extraordinary VSP, which period is about 416 ms, W_p is about 35 – 60 ms, and W_g is about 365 – 380 ms.

Among 40 VSPs associated with the flare/CME event, there are only 3 extraordinary VSPs, which occurred at 03:25:40 – 03:25:47 UT, 03:28:10 – 03:28:15 UT, and 03:44:09 – 03:44:14 UT, and their periods are 416 ms, 200 ms, and 160 ms, respectively. All extraordinary VSPs belong to slow-VSP, strongly right circular polarization, and the magnitude of the pulsating emission flux is in the range of 30 – 70 sfu.

In fact, all of the QPPs can be also classified into ordinary QPP and extraordinary QPP. When we re-scrutinize the scales of W_p and W_g in other QPPs, we may find that almost all the VLP, LPP, and SPP are belonging to ordinary QPP.

3.5. Relationships among QPPs in Multi-timescales

Fig.10 presents a synthetical comparison of temporal relationships of the 5 classes of QPPs with different timescales, GOES soft x-ray flux, and the transport rate of magnetic helicity (dH/dt). We find that all LPPs and SPPs occurred near peaks of VLP. Additionally, from the flare impulsive phase to its decay phase, the duration of LPP is gradually decreased. However, VSPs distribute in all phases of the flare (rising phase, peak, decay phase, or vale). And this may imply that VSP is possibly independent from other classes of QPPs. It seems to be a small additional component superposed on other classes of QPPs with longer timescales.

The period ratios between different QPPs may be meaningful. Around the first LPP shown in Fig.10, there occurred 3 classes of QPPs: VLP (paragraph A), LPP and SPP. Their averaged periods are 4.13 min, 70 s, and 8 s, respectively. Their ratios are 31.0 : 8.75 : 1. The second LPP is just occurred in the gap between paragraph A and B of VLP, and during this gap we did not distinguish other kind of QPP. During the third LPP, there occurred VLP (paragraph A, $P = 4.5$ min), LPP ($P = 15$ s) and VSP ($P = 90 \sim 110$ ms). The period ratio is about 2700 : 150 : 1, which is entirely different from the former ratios. Fig.11 shows an example of concurrence of two different classes of QPPs occurred at 02:38:50 – 02:40:00 UT. The higher hierarchy of QPP is a LPP with period of 16 s, and the lower hierarchy of QPP is a fast-VSP with period of 77 ms. From this figure we find that the LPP is fine-structured with a train of fast-VSPs, and the period ratio is more than 200. And in the train of fast-VSPs, we find that there is obviously global frequency drifting rate with value of about 2.5 MHz/s, and this drift rate is very slow comparing with the single pulse frequency drifting rates. These evidences imply that there is no obvious regulations among the period ratios and the weakly links between the different classes of QPPs.

Additionally, from careful investigation of the microwave observations there is no evidence of any LPP, SPP and VSP found around the time intervals of VLP paragraph C and D. It seems that all the LPP, SPP, and VSP take place around the time intervals of VLP paragraph A and B.

Usually, the microwave burst can be regarded as a prompt signal of non-thermal energetic particles originating from the magnetic reconnection. So it is meaningful to quest for the relationships between the magnetic field and QPPs. Here, we introduce the transport rate of magnetic helicity (dH/dt) to describe the magnetic field behavior. It can be expressed as (Berger & Field, 1984):

$$\frac{dH}{dt} = \oint 2(\mathbf{B} \cdot \mathbf{A}_p)v_z dS - \oint 2(\mathbf{v} \cdot \mathbf{A}_p)B_z dS.$$

Here, \mathbf{A}_p is magnetic vector potential, v is the fluid velocity, and B_z is the normal component of the

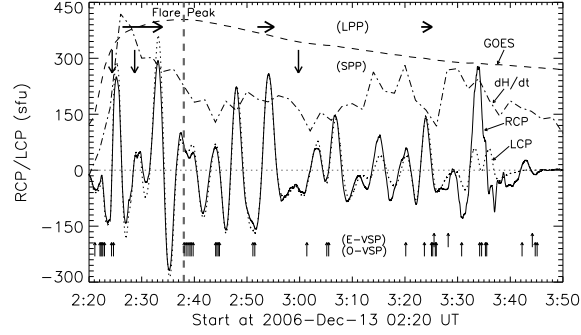


Fig. 10.— A synthetical comparisons of the temporal relationships among the 5 classes of QPPs, GOES soft x-ray flux (GOES), and the transport rate of magnetic helicity (dH/dt). Profiles of the left- and right-circular polarization (LCP, RCP) represent the VLP, while the big, moderate and vertical small arrows represent LPP, SPP, and VSP, respectively. The length of the big arrow show the duration of LPP. Here O-VSP indicates the ordinary VSP, and E-VSP indicates the extraordinary VSP.

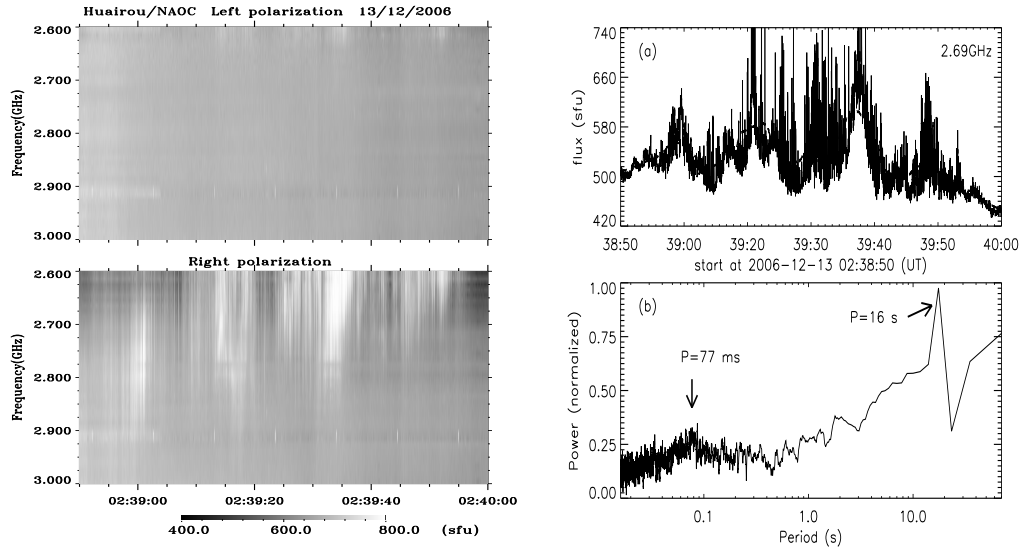


Fig. 11.— An example of concurrence of two different hierarchies of QPPs. The left panel is the spectrograms of left- and right-circular polarization. Panel (a) is a flux curve at frequency of 2.69 GHz, the solid curve indicates a fast-VSP, and the thick-dashed curve indicates a LPP. Panel (b) is a result of Fast Fourier Transformation at frequency of 2.69 GHz, the two peaks represent a VSP of period 77 ms and a LPP of period 16 s, respectively.

magnetic field. In an open volume, the magnetic helicity may change by the passage of helical magnetic field lines through the surface (the first term) and by shuffling horizontal motion of field lines on the surface (the second term). In an isolated active region dH/dt is a nonpotential parameter which indicates the dynamic evolution of the magnetic field mainly in the flaring region (Berger & Field, 1984). As the flare/CME event occurred in an isolated active region of AR 10930, we may estimate the quantity for the event by calculating from the above expression. The work of Zhang et al (2008) presents that the temporal profile of dH/dt is consistent with that of microwave burst in the flare/CME event on Dec.13, 2006. So we superposed the curve of dH/dt in the same duration in Fig.10 (dashed-dotted curve). Here, the cadence of dH/dt is 2 minutes, which is calculated from the observations of the Solar Optical Telescope on board Hinode (SOT/Hinode, Tsuneta et al, 2008; Kosugi et al, 2007). From the comparison of dH/dt and QPPs, we find that when QPPs take place dH/dt is positive. This fact indicates a continuous injection of magnetic helicity. This may lead to accumulation of nonpotential energy and the magnetic reconnections in the flaring active region. There are some variations in the profile of dH/dt during the flaring event. However, as the cadence of dH/dt is only 2 minutes, we could not confirm any pulsating features in dH/dt .

Actually, we find that VLP, LPP and SPP have much of similarities, such as broad emission bandwidth, almost at the same level of Q-factor (≤ 10), weakly circular polarization, and relatively slow frequency drift rates, except that they have different durations, periods, and different magnitude of pulsating emission flux. They belong possibly to a same class of QPP in a sense. In order to confirm such viewpoint, we plot all the QPPs in a logarithmic period-duration space in Fig.12. We find that all of the VLPs, LPPs, SPPs, and part of slow-VSPs are distributed around a line. However, almost all fast-VSPs and most part of the slow-VSPs are distributed far away from the above line dispersively. This fact implies that fast-VSPs and part of slow-VSPs may be different originally from VLPs, LPPs, and SPPs. Hereby, we may classify all QPPs into two groups: group I includes VLPs, LPPs, SPPs, and part of slow-VSPs of which the longer the duration corresponds to the longer period; group II includes fast-VSPs and most part of slow-VSPs of which the period is dispersive respect to the duration.

Table 2 presents a brief summary of VLP, LPP, SPP, slow-VSP, and fast-VSP.

Table 2: A brief summary of QPP with different timescales. Max-F indicates the magnitude of pulsating emission flux at each pulse in QPP

| Hierarchy | VLP | LPP | SPP | slow-VSP | fast-VSP |
|--------------------|-------------|-------------|--------------|--------------|-------------|
| D(s) | 1140 ~ 2640 | 90~450 | 20~80 | 2.2 ~ 23 | 2.3 ~ 16 |
| Max-F(sfu) | 90 ~ 1200 | 70 ~ 220 | 40~115 | 20 ~ 95 | 15 ~ 70 |
| b_w (MHz) | > 1200 | > 1200 | ~ 900 | 250 ~ 700 | 220 ~ 400 |
| Mean period(s) | 220~270 | 15 ~ 70 | 1.2 ~ 8 | 0.11 ~ 0.416 | 0.021~ 0.09 |
| r(%) | 8 ~ 45 | 10 ~ 20 | 45 ~ 65 | 45 ~ 60 | 55 ~ 75 |
| Q-factor | 6 ~ 10 | 5 ~ 7 | 4 ~ 10 | 12 ~ 209 | 30 ~ 275 |
| R_{spdf} (MHz/s) | -440 ~ 389 | -610 ~ 78.5 | -4000 ~ 3500 | 6500~20000 | 8330~>30000 |
| Cases | 4 | 4 | 3 | 10 | > 30 |

4. Discussion of the Physical Mechanisms

From above investigations, we find that there are 5 classes of QPPs with different timescales associated with the flare/CME event: VLP, LPP, SPP, slow- and fast-VSP. They form a broad hierarchy of timescales of hecto-second, deca-second, a few seconds, deci-second, and centi-second. And this is similar to the discovery of microwave burst timescales by Kruger et al (1994). They classified the microwave burst timescales as tens of minutes, a few minutes, a few seconds and sub-seconds which represent to main burst phase, main burst pulse, subpulse and spiky burst elements, respectively. But, these bursts have no obvious periodicities. However, our investigations indicate that the most remarkable feature of QPPs is the quasi-periodicity of the repetitive pulses. Then, what is the generation mechanism of the above various classes of QPPs?

It is well known that harmonic motion of a classic mechanic oscillator is due to a restoring force proportional to the displacement, and any elastic body can be excited to oscillate in eigen-modes. When a magnetic field presents in plasma systems, the characteristic eigen-frequencies will be determined by the magnetic field, plasma density, temperature, and geometrical configurations of the magnetized plasma system. Aschwanden (1987) presented an extensive review of pulsation models and classified them as three groups:

(1) MHD flux tube oscillations, which modulate the radio emissivity with a standing or propagating MHD waves, e.g. slow magnetoacoustic mode, fast kink mode, fast sausage mode (Roberts, Edwin & Benz, 1984; Nakariakov & Melnikov, 2009).

(2) Periodic self-organizing systems of plasma instabilities of wave-particle or wave-wave interactions interlocked by a Lotka-Volterra type of coupled equations (Aschwanden & Benz, 1988).

(3) Modulation of periodic acceleration (repetitive injection of particles into the emission source region) which may possibly generated from repetitive magnetic reconnections, for example, the pulsed acceleration in solar flare (Aschwanden et al, 1994; Aschwanden, 2004) or the multi-scale cascading reconnection processes in the current sheet (Kliem et al, 2000; Karlicky et al, 2005).

4.1. VLP Mechanism

At first, we investigate the generation mechanism of VLP. From Table 1 we know that periods of VLPs are 220 – 270 s, they are very similar to the oscillations obtained by Aschwanden et al (1999) from the TRACE 171Å observations. In that case the period of oscillations is 276 s, and they interpret them as a standing fast kink mode and might be a resonant coupling with the photospheric 5-min p-mode oscillations. The period is expressed as:

$$P_{kink}^{fast} = \frac{2L}{sc_k} = \frac{4\pi^{1/2}L}{s} \left(\frac{\rho_o + \rho_e}{B_o^2 + B_e^2} \right)^{1/2} \simeq 6.48 \times 10^{-17} \frac{L\sqrt{n_e}}{B}. \quad (1)$$

Here, the number of nodes is $s - 1$, $c_k = \left(\frac{\rho_o v_A^2 + \rho_e v_{Ae}^2}{\rho_o + \rho_e} \right)$ is the mean Alfvén speed for the inhomogeneous medium, L is the loop length (m), $\rho = n_i m_i$ is the plasma density and subscript o and e refer to inside and outside of the loop, $n_i \sim n_e$ (m^{-3}), the magnetic field B is in Tesla.

In our case, the active region AR 10930 is an isolated one on the solar disk during about 20 days before and after the flare event (Fig.13). And it is structured mainly in two big sunspots, the leading sunspot (marked as A in Fig.13) is about $50''$ (about 36,000 km), and the diameter of the following sunspot (marked

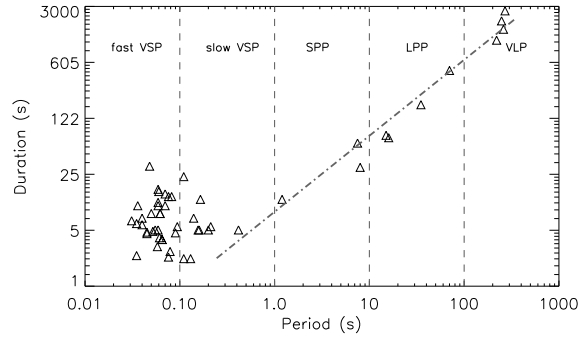


Fig. 12.— Relationship between the duration and the periods of QPPs. Each triangle denotes one QPP case, and the dot-dashed line is linear fitted.

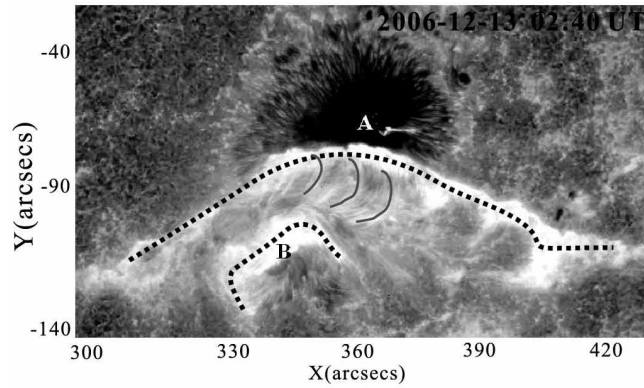


Fig. 13.— Skeleton map of the active region AR 10930 observed by Ca II H line on SOT/Hinode around the flare peak (2006-12-13, 02:40 UT). The thick black dotted lines indicate the flare ribbons, and the red solid lines sketched part of the small bright flux loops. A is the leading sunspot, and B is the following rotating sunspot.

as B in Fig.13) is about 15,000 km. Over these two sunspots there are many loops which connect from one sunspot to the other. We may assume that the foot-points are located near ribbons (the thick black dotted lines in Fig.13). Then we can estimate the lengths of loops. The distance between two ribbons is in the range of $19.5'' - 39''$, that is about 14 - 28 Mm. Suppose loops are semicircles, the loop lengths are $L = 44 - 88$ Mm. The plasma density and magnetic field strength of the emission source region are estimated as $B \sim 50 - 200$ G, $n_e \sim 10^{11} \text{ cm}^{-3}$ (Yan, et al, 2007). Based on these parameters and Equ.(1) we obtain that the period is in the range of 9.0 - 36 s. Even if we suppose the estimation with variation by a factor of 4, it is also in the range of 2.5 - 144 s, too short to fit the observed periods of VLP. Periods of standing fast sausage mode or propagating MHD mode are shorter than that of standing fast kink mode, they are not possible to be the candidate mechanism of VLPs.

Then what about the standing slow MHD modes? We know that both of the standing slow sausage mode and standing slow kink mode have periods:

$$P_{slow} = \frac{2L}{sc_T} = \frac{2L}{sc_0} [1 + (\frac{c_0}{v_A})^2]^{1/2} \approx 1.30 \times 10^{-2} \frac{L}{\sqrt{T_e}}. \quad (2)$$

Here $c_T = c_0 v_A / (c_0^2 + v_A^2)^{1/2}$ is the tube speed in magnetic flux tube, c_0 is the sound speed, v_A the Alfvén speed, T_e (K) is the temperature in the plasma loop. We may use the brightness temperature to replace the plasma temperature approximately:

$$T \sim T_B = \frac{c^2 D^2 F}{k_B f^2 r^2} \approx 1.46 \times 10^{40} \frac{F}{f^2 r^2}. \quad (3)$$

Here c is the speed of light, D is the distance between the Sun and the Earth, F is the microwave emission flux intensity in unit of sfu, r is the radius of the emission source region in unit of m. As the microwave flux intensity (F) is from the whole sun, which may include a multiple loop sources. So, we may suppose that the emission source of F will be reasonably as the size of whole active region, i.e. the size of AR 10930, which will be about $r = 2 \times 10^5$ km. When $f = 3.2$ GHz, the mean microwave flux intensity $F = 300$ sfu, then $T \sim 1.22 \times 10^7$ K. Then we may gain the period is 186.4 - 372.6 s, which is very close to the observed result of VLPs. So, we suggest that VLPs are possibly generated from standing slow MHD modes.

Fig. 4 and Table 1 indicate that the magnitude of the pulsating emission flux of VLP is in the range of 90 - 1200 sfu, which is very strong modulation. In fact, each pulse of the VLPs is very like a small eruptive process. We know that the kink mode can change the magnetic field by altering the direction. But it can change neither the magnitude of the magnetic field, nor the plasma density of the loops directly. It is not clear how kink mode produce so strong modulation of the microwave emissions. We would rather believe that the VLP is generated by a standing slow sausage mode.

On the other hand, Kosovichev and Sekii (2007) found that solar umbra of the leading sunspot had a 3-min oscillation which started immediately after the hard X-ray peak (50 - 100 keV in RHESSI) and just before the soft X-ray maximum (GOES-12), with the amplitude exceeding to that of pre-flare oscillations by a factor of 2 - 4. However, at the same time Kosovichev and Sekii (2007) also pointed out that the 3-minute umbra oscillation is uncertainty because of the poorly observation cadence. As the periods of VLPs are 220 - 270 s, which are very close to the periods of the photospheric 5-min p-mode oscillations ($P = 220 - 400$ s), we are apt to believe that Kosovichev and Sekii (2007) underestimated the periods of the umbra oscillations of the leading sunspot. The authors prefer to deduce that VLP is a result of standing slow sausage mode

coupling and resonating with the underlying photospheric 5-min p-mode oscillations. The modulation is amplified and constructs the main framework of the whole flare/CME eruptive processes.

4.2. LPP and SPP Mechanism

Fig.12 indicates that almost all of VLPs, LPPs, SPPs, and part of slow-VSPs are distributed around a line in the logarithmic period-duration space, they are in a same QPP group. It is also reasonable to suppose that LPP, SPP and part of slow-VSP have a generating mechanism similar to that of VLP, at least they are also generated from some MHD modulations. From Equ.(1) we get the period in the range of 2.5 - 144 s, which is consistent with the observed results of LPPs. Hence the standing fast kink mode may be the most possible candidate mechanism of LPP.

As for SPP, the standing fast kink mode might be a weakly candidate. The standing fast sausage mode should be the much preferential mechanism. Its period is:

$$P_{sausage}^{fast} = \frac{2\pi a}{c_k} \approx 2.02 \times 10^{-16} \frac{a\sqrt{n_e}}{B}. \quad (4)$$

a is the loop width (m). From Fig.13 we may estimate the loop width as about $1'' - 3''$, i.e. 700 - 2000 km. Then the period is 2.2 - 25.6 s. If the estimation has a variation by a factor of 4, it is in the range of 0.6 - 100 s, which includes the whole range of SPP and possibly LPP.

Actually, the propagating MHD mode have a period of a factor of 0.6 shorter than that of standing fast sausage mode. With the parameters in our case, the period is in the range of 0.4 - 60 s. Hence the propagating MHD mode is also a possible mechanism of LPP and SPP.

Additionally, from Equ.(1) and Equ.(4) we may find that the periods are most strongly dependent on the scales of the loop (length or section radius). AR 10930 is a complex active region, it is most possible that there is a variety of plasma loops of which the scales are smaller than the above estimation. With such smaller scale plasma loops, the periods of the standing fast kink modes or the standing fast sausage modes are most likely to extend to second and even sub-second, which may explain the mechanism of LPP, SPP, and part of slow-VSP.

There is another alternative mechanism for the QPP with periods $P > 1$ s. Zaitsev et al (1998, 2000) proposed that a coronal loop can be twisted and then carries an electric current. This current-carrying plasma loop becomes a LRC-circuit resonator, and the circuit oscillations can cause periodic modulation of loop magnetic field, energy release rate and electron acceleration, therefore, the emission of non-thermal electrons (Khodachenko et al, 2005; Khodachenko et al, 2009). The eigen oscillation of the LRC-circuit resonator may be a possible mechanism of microwave QPP. When the electric resistance can be neglected, the period of the circuit oscillations is:

$$P_{LRC} = \frac{2\pi}{c} \sqrt{L\mathcal{C}} \sim \frac{10^{12}}{I_\varphi}. \quad (5)$$

Here, $L = 4l(\log \frac{8l}{a\pi} - \frac{7}{4})$ is the loop inductance, $\mathcal{C} = \frac{c^4 \rho S^2}{2\pi l I_\varphi^2}$ is the effective loop capacitance. $S = \pi a^2$, a is the loop section radius (m), l is the loop length (m), ρ is the plasma mass density. I_φ is the longitudinal electric current (A) in the loop. The LRC-circuit model has been applied to explain the microwave pulsation

with periods of 0.7 – 17 s (Zaitsev et al, 1998). Observations show that the longitudinal electric current is possibly in the range $2.87 \times 10^{10} - 3.462 \times 10^{12}$ A (Tan, 2007, etc), then we obtain the oscillation period is about 0.3 – 35 s, which is due to LPP or SPP, and part of slow-VSP.

4.3. VSP Mechanism

Different from VLPs, LPPs, SPPs, and part of slow-VSPs (Group I), the fast-VSP and the most part of slow-VSP are attributed to another group (Group II), dispersively distributed away from the line (Fig.12). This implies that the generation mechanisms of fast-VSP and part of slow-VSP are intrinsically different from Group I. In the work of Tan et al (2007) and Tan (2008), VSP is explained as a result of modulations of the resistive tearing-mode oscillations in some electric current-carrying flare loops, and the pulsating emission is explained as plasma emission. The period is:

$$P_{tear} = \frac{4\pi^2 a^2 \sqrt{\rho}}{I_\varphi \sqrt{M \mu_0}} \approx 1.44 \times 10^{-9} \frac{a^2}{I_\varphi} \sqrt{\frac{n_e}{M}}. \quad (6)$$

Here, M is a parameter related to the distribution of the electric current in plasma loop and the mode numbers of the tearing-mode perturbations. μ_0 is the permeability of free space. From Fig.6 of Tan et al (2007), we know that P_{tear} can produce almost all kinds of VSPs with period of sub-seconds.

Additionally, the duration of quasi-periodic pulsating structure is $D \simeq 0.1513 \left(\frac{\Delta'}{j m B_\theta}\right)^{2/3} t_A^{2/3} t_r^{1/3}$ (Tan, 2008), here Δ' is the tearing mode instability factor, m is the mode number, t_A the Alfvén time scale (unit of second), t_r the resistive diffusive time scale (unit of second), j the current density (unit of $A m^{-2}$), and B_θ is the radial derivation of the poloidal magnetic field. We may obtain the duration is about 200-300 s, which is much longer than the observed durations (2.2-23 s). The most possible reason is that there are many loops participating in the eruptive processes in the flaring region, and the pulsating structure is evident only when the contribution coming from a single flare loop. If the contribution comes from several loops, the pulsating structure will become diffuse or disappear because of superposition or interference. So, our observations of VSPs are always fractional sections.

The duration is dominated by the current density distribution, magnetic configuration and plasma resistivity, while the period of pulsation is dominated by the total electric current, the loop's geometrical parameters, and the distribution of current density in the cross-section. At the same time, the pulsating emission is localized in some regions with small size, for example, localized around magnetic islands in flaring plasma loops. From the bandwidth of the emission we may estimate the perturbation of the plasma density. From the frequency drifting rate we may estimate the motion of the plasma loop and the motion of the energetic particles. Combining all these observable parameters, we may probe almost all the physical conditions and their evolutions.

In a word, the long period pulsation is possibly associated with a large scale magnetized-plasma loop, while the short period pulsation is possibly associated with some small scale configuration in solar corona. The very short period pulsation may reflect some local information about flaring plasma loops.

On the other hand, as all extraordinary VSPs are occurred essentially after the main burst of the flare/CME event, we may adopt the load/unload model (Nakariakov and Milnikov, 2009) to interpret them. In load/unload model, QPP is a side effect of transient energy releases, and the period is determined by a buildup of free energy, the mechanism of the energy release, and the energy outflow rate. We may suppose

that energy release mechanism is magnetic reconnection which is instantaneous and short-lived, and energy outflow rate is determined by the magnetic configurations which does not change observably after the main burst of the flare/CME event. Then the period of QPP will be determined mainly by the buildup of free energy. Naturally, very after the main burst of the flare/CME event, the source region becomes exhausted. So, the buildup of the free energy will take a long time, the energy release lasts much less time, and cause $W_p \gg W_g$. The strongly right circular polarization indicates that the emission source arises in some small places with simplex magnetic configurations.

5. Summary

From investigations in this work, we obtain following conclusions: the timescales of microwave QPPs are distributed in a broad range from hecto-second (VLP), deca-second (LPP), a few second (SPP), deci-second (slow-VSP) to centi-second (fast-VSP), associated with the X3.4 flare/CME event of 2006 December 13 in active region AR 10930. These QPPs are occurred successively around this event and form a broad hierarchy. The higher hierarchy of QPP has longer periods and durations, higher magnitude of the pulse emission fluxes, wider frequency bandwidth, and weaker circular polarized, lower frequency drift rates; while the lower hierarchy of QPP has shorter periods and durations, lower magnitude of the pulse emission fluxes, narrower frequency bandwidth, and stronger circular polarized, higher frequency drift rates.

In logarithmic period-duration space, VLP, LPP, SPP, and part of slow-VSP are approximately distributed around a line which implies that all of them have the similar generation mechanism. Fast-VSP and the most part of slow-VSP depart far from the above line which implies that they possibly have different mechanisms.

Estimations show that VLP is possibly resulted from the standing slow sausage modes coupling and resonating with the underlying photospheric 5-min p-mode oscillations. It may be associated with evolutive behaviors of the solar internal structures. As VLPs have the largest magnitude of emission fluxes, we suggest that the modulations are amplified and form the main framework of the whole flare/CME eruptive processes. From Equ.(2) and (3), we can estimate the radius of the emission source region:

$$r \simeq 9.3 \times 10^{21} \frac{P}{fL} F^{\frac{1}{2}}. \quad (7)$$

Here, the period (P), radio central frequency (f) and radio emission intensity (F) can be obtained from radio observations, the loop length (L) can be estimated from the optical or other imaging observations approximately. Then we may obtain the radius of the radio emission source region (r) by adopting Equ.(7) even if we have no radio imaging observations. By substituting the parameters obtained in the above sections, we may get the radius of the emission source region from VLP paragraph A, B, C to D is from 2.04×10^5 km, 2.06×10^5 km, 1.62×10^5 km to 0.92×10^5 km, i.e., the source region is undergoing an evolutive process of expanding at first, and then shrinking. However, as we have no radio imaging observations at the corresponding frequencies, we do not know the exact cites of the emission source region, the only thing we can do is to adopt the averaged loop length in our above estimations, which may have much uncertainties.

Similar to VLP, LPP and SPP (may include part of slow-VSP) are also caused by MHD oscillations. However, their MHD modes may have some differences. They may be related with the standing fast sausage or kink modes. The propagating MHD modes and the LRC-circuit resonance of current-carrying plasma loops are also the possible candidates of the generating mechanism.

Fast-VSP and most part of slow-VSP are generated by a completely different mechanism: the modulation of the resistive tearing-mode oscillations in electric current-carrying flare loops. In this mechanism, both, the period and duration of QPP are coupled with the magnetic field, plasma density, electric current, and the loop parameters. By using their relation, we may deduce the physical conditions of the emission source region.

The timescale of periods of QPPs implies a limit on the pulsating emission source size. Regardless of generating mechanism the pulsating source must be smaller than that given by the product of speed of light and period (P). If not, the pulsating structure would be smeared out (Elgarøy, 1986). So, it is reasonable to suppose that the short periodic QPP may come from a smaller source region. The broad hierarchy of timescales of QPPs occurred in a flare event may imply that there is a multi-scale hierarchy of sizes of the magnetic configurations in the flaring region, and timescales of the dynamic processes. The frequency drift rate and the bandwidth of the pulsating emission are dominated by the emission mechanism which is always related to the magnetic field strength, plasma density, and possibly to the plasma temperature. It may be reasonable to suppose that the frequency drift features of QPPs implies the motion of the pulsating source regions, and the bandwidth of the pulsating emission are related to the dimensional size of the pulsating source regions.

The period ratio between different classes of QPP have no obvious trend. This fact may imply that there is no originated link between different classes of QPP, even if they are occurred simultaneous in the same frequency range. Actually, it is possible that the short periodic QPP (e.g. fast-VSP, etc) is a small quasi-periodic perturbation which superposed on the longer periodic QPPs (e.g. VLP, etc), and the latter may dominate the whole evolution of the flaring processes.

However, so far, because of the lack of imaging observations with spatial resolutions in the corresponding frequency range, there are many unresolved problems of the QPPs, for example, the spatial behaviors, the spatial scales of the source region, etc. To overcome such problems, we need some new instruments, for example, the constructing Chinese Spectral Radioheliograph (CSRH, 0.4 - 15 GHz) in the decimetric to centimeter-wave range (Yan et al, 2009) and the proposed American Frequency Agile Solar Radiotelescope (FASR, 50 MHz - 20 GHz) (Bastian, 2003). Maybe, when these instruments begin to work, we can get more and more cognitions of the solar eruptive processes.

The authors would like to thank the referee's friendly and valuable comments on the paper. Baolin Tan's work is supported by NSFC Grant No. 10733020 and 10873021, Yin Zhang's work is supported by NSFC Grant No. 10903013. This work is also partly supported by MOST Grant No. 2006CB806301 and CAS-NSFC No. 10778605.

REFERENCES

- Abrami, A.: 1970, *Solar Phys.* **11**, 104.
- Aschwanden, M.J., & Benz, A.O.: 1986, *Astron. Astrophys.* **158**, 102.
- Aschwanden, M.J.: 1987, *Solar Phys.* **111**, 113.
- Aschwanden, M.J., & Benz, A.O.: 1988, *Astrophys. J.* **332**, 466.

- Aschwanden, M.J., Benz, A.O., Dennis, B.R., & Kundu, M.R.: 1994, *Astrophys. J. Suppl.* **90**, 631.
- Aschwanden, M.J., Fletcher, L., Schrijver, C.J., & Alexander, A.: 1999, *Astrophys. J.* **520**, 880.
- Aschwanden, M.J.: 2004, *Astrophys. J.* **608**, 554.
- Bastian, T.: 2003, *Proc. SPIE.* **4583**, 98.
- Benz, A.O., Gudel, M., Isliker, H., Miszkowicz, S. & Stehling, W.: 1991, *Solar Phys.* **133**, 385.
- Berger, M.A., & Field, G.B.: 1984, *J. Fluid Mech.* **147**, 133.
- Dulk, G.A.: 1985, *Ann. Rev. Astron. Astrophys* **23**, 169.
- Elgarøy, ϕ .: 1986, *Solar Phys.* **104**, 43.
- Fleishman, G.D., Fu, Q.J., Wang, M, Huang, G.L. & Milnikov, V.F.: 2002, *Phys. Rev. Lett.* **88**, 251101.
- Foullon, C., Verwichte, E., Narkariakov, V.M., & Fletcher, L.: 2005, *Astron. Astrophys.* **440**, L59.
- Foullon, C., Fletcher, L., Hannah, I.G., Verwichte, E., Cecconi, B., Narkariakov, V.M., Phillips, K.J.H., & Tan, B.L.: 2010, *Astrophys. J.* **719**, 151.
- Fu, Q.J., Qin, Z.H., Ji, H.R., & Pei, L.B.: 1995, *Solar Phys.* **160**, 97.
- Fu, Q.J., Ji, H.R., Qin, Z.H., et al: 2004, *Solar Phys.* **222**, 167.
- Gotwols, B.L.: 1972, *Solar Phys.* **25**, 232.
- Inglis, A.R., & Nakariakov, V.M.: 2009, *Astron. Astrophys.* **493**, 259.
- Jiricka K., Karlicky M., Kepka, O., & Tlamicha, A.: 1993, *Solar Phys.* **147**, 203.
- Jiricka K. & Karlicky M.: 2008, *Solar Phys.* **253**, 95.
- Kaufmann, P.: 1972, *Solar Phys.* **23**, 178.
- Karlicky, M., Barta, M., Meszarosova, H., & Zlobec, P.: 2005, *Astron. Astrophys.* **432**, 705.
- Karlicky, M., Zlobec, P., & Meszarosova, H.: 2010, *Solar Phys.* **261**, 281.
- Khodachenko, M.L., Zaitsev, V.V., Kislyakov, A.G., Rucker, H.O., & Urpo, S.: 2005, *Astron. Astrophys.* **433**, 691.
- Khodachenko, M.L., Zaitsev, V.V., Kislyakov, A.G., & Stepanov, A.V.: 2009, *Space Sci. Rev.* **149**, 83.
- Kliem, B., Karlicky, M., & Benz, A.O.: 2000, *Astron. Astrophys.* **360**, 715.
- Kosovichev, A.G., & Sekii, T.: 2007, *Astrophys. J.* **670**, L147.
- Kosugi, T., Matsuzaki K., Sakao, T., & et al: 2007, *Solar Phys.* **243**, 3.
- Kruger, A., Kliem, B., Hildebrandt, J, & Zaitsev, V.V.: 1994, *Astrophys. J.* **90**, 683.
- Kubo, M., Yokoyama, T., Katsukawa, Y, et al: 2007, *Publ. Astron. Soc. Japan* **59**, S779.
- Kuznetsov, A.A.: 2008, *Solar Phys.* **253**, 103.

- Ma, Y., Xie, R.X., Zheng, X.M., & Yan, Y.H.: 2006, *Chin. Astron. Astrophys.* **30**, 303.
- Melnikov, V.F., Reznikova, V.E., Shibasaki, K., & Nakariakov, V.M.: 2005, *Astron. Astrophys.* **439**, 727.
- Minoshima, T., Imada, S., Morimoto, T., Kawate, T., Koshiishi, H., Kubo, M., Inoue, S., Isobe, H., Masuda, S., Krucker, S & Yokoyama, T.: 2009, *Astrophys. J.* **697**, 843.
- Nakariakov, V.M., & Milnikov, V.F.: 2009, *Space Sci. Rev.* **149**, 119.
- Nakariakov, V.M., Foullon, C., Myagkova, I.N., & Inglis, A.R.: 2010, *Astrophys. J.*, **708**, L47.
- Ning, Z.J.: 2008, *Solar Phys.* **247**, 53.
- Parks, G.K., & Winchler, J.R.: 1969, *Astrophys. J.* **155**, L117.
- Qin, Z.H., Li, C.S., Fu, Q.J., & Gao, Z.M.: 1996, *Solar Phys.* **163**, 383.
- Roberts, B., Edwin, P.M., & Benz, A.O.: 1984, *Astrophys. J.* **279**, 857.
- Rosenberg, H.: 1970, *Astron. Astrophys.* **9**, 159.
- Sawant, H.S., Subramanian, K.R., Faria, C., et al: 2001, *Solar Phys.* **200**, 167.
- Su, Y.N., Golub, L., Van Ballegoijen, A, et al: 2007, *Publ. Astron. Soc. Japan* **59**, S785.
- Tan, B.L.: 2007, *Adv. Space Res.* **39**, 1826.
- Tan, B.L., Yan, Y.H., Tan, C.M., & Liu, Y.Y.: 2007, *Astrophys. J.* **671**, 964.
- Tan, B.L.: 2008, *Solar Phys.* **253**, 117.
- Tanaka, H., Castelli J.P., Covington A.E., et al: 1973, *Solar Phys.* **29**, 243.
- Trottet, G., Kerdraon, A., Benz, A.O., & Treumann, R.: 1981, *Astron. Astrophys.* **93**, 129.
- Tsuneta, S., et al: 2008, *Solar Phys.* **249**, 167.
- Wang, M., & Xie, R.X.: 2000, *Chin. Astron. Astrophys.* **24**, 95.
- Yan, Y.H., Tan, C.M., Xu, L., Ji, H.R., Fu, Q.J., & Song, G.X.: 2002, *Sci. Chin. A Suppl.* **45**, 89.
- Yan, Y.H., Huang, J., Chen, B., & Sakurai, T.: 2007, *Publ. Astron. Soc. Japan* **59**, 815.
- Yan, Y.H., Zhang, J., Wang, W., Liu, F., Chen, Z.J., & Ji, G.S.: 2009, *Earth. Moon. Planet* **104**, 97.
- Young, C.W., Spencer, C.L., Moreton, G.E., & Roberts, J.A.: 1961, *Astrophys. J.* **133**, 243.
- Zaitsev, V.V., & Stepanov, A.V.: 1982, *Sov. Astron. Lett.* **8**, 132.
- Zaitsev, V.V., Stepanov, A.V., Urpo, S., & Pohjolainen, S.: 1998, *Astron. Astrophys.* **337**, 887.
- Zaitsev, V.V., Urpo, S., & Stepanov, A.V.: 2000, *Astron. Astrophys.* **357**, 1105.
- Zhang, Y., Tan, B.L., & Yan, Y.H.: 2008, *Astrophys. J.* **682**, L133.